INTERNATIONAL JOURNAL OF PHARMACEUTICAL SCIENCES
[ISSN: 0975-4725; CODEN(USA): IJPS00]
Journal Homepage: https://www.ijpsjournal.com

OPEN ACCESS

Research Article

Decoding the Cardioprotective Effects of *Grewia hirsuta*: A Computational and Experimental Approach

Aditi Malkar*, Karna Khavane, Aditi Jyotishi

Dr. Vedprakash Patil Pharmacy College, Aurangabad

ARTICLE INFO

Published: 28 Jul. 2025
Keywords:
Cardioprotective effect, Grewia hirsuta Vahl, heart, Electrocardiograms, Cardiovascuclar diseases, DOX-induced cardiotoxicity
DOI:
10.5281/zenodo.16537277

ABSTRACT

Cardiovascular diseases (CVDs) remain a predominant global health burden, with heart failure constituting a major cause of morbidity and mortality. Among the various risk factors contributing to cardiac dysfunction, drug-induced cardiotoxicity has garnered significant attention due to its impact on long-term cardiac health. The scientific validation of Grewia hirsuta as a cardioprotective agent against DOX-induced cardiotoxicity is essential for multiple reasons. Firstly, addressing the unmet need for effective cardioprotective agents is critical, as the currently available strategies for managing DOX-induced cardiotoxicity, such as dexrazoxane and angiotensin-converting enzyme (ACE) inhibitors, have notable limitations. Dexrazoxane, the only FDA-approved agent for reducing DOX-induced cardiotoxicity, is often associated with concerns regarding potential interference with chemotherapy efficacy and the risk of secondary malignancies. This study not only has the potential to impact the field of cardioprotection but also offers broader implications for integrative medicine, where natural products are increasingly being recognized as valuable therapeutic agents. If successful, the identification of Grewia hirsuta as a cardioprotective agent could pave the way for future clinical trials and translational research aimed at incorporating natural compounds into mainstream oncology and cardiology practice.

INTRODUCTION

The Human Heart: Structure and Function

Internally, the heart is divided by a muscular septum into right and left halves, each comprising an atrium and a ventricle. The right atrium receives deoxygenated blood from the superior and inferior vena cava, as well as the coronary sinus. This blood passes through the tricuspid valve into the right ventricle, which pumps it into the pulmonary artery via the pulmonary valve for oxygenation in the lungs. On the left side, oxygenated blood from the lungs enters the left atrium via the pulmonary

***Corresponding Author:** Aditi Malkar
Address: *Dr. Vedprakash Patil Pharmacy College, Aurangabad.*
Email : aditimalkar15@gmail.com
Relevant conflicts of interest/financial disclosures: The authors declare that the research was conducted in the absence of any commercial or financial relationships that could be construed as a potential conflict of interest.

veins and flows into the left ventricle through the mitral valve. The left ventricle then contracts to deliver blood into the aorta through the aortic valve, initiating systemic circulation. Notably, the left ventricular wall is considerably thicker than the right due to the higher pressure needed to pump blood throughout the body. (Anderson et al., 2004; Ellis, 2012; Zhong et al., 2020)

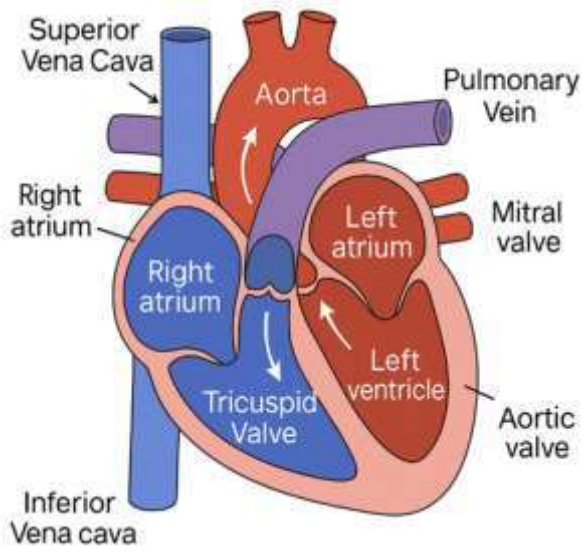

Figure 1: Anatomy of human heart

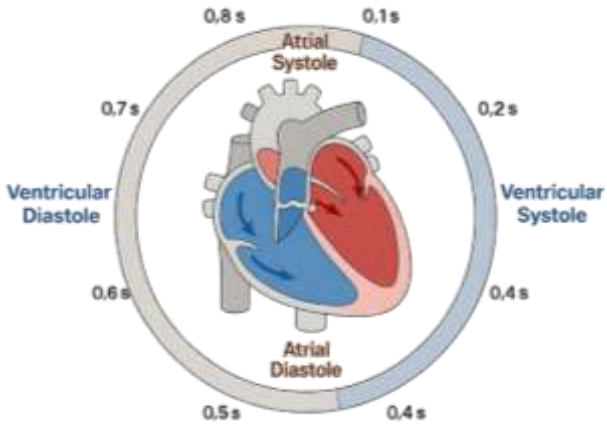

Figure 2: The Cardiac Cycle Timeline Depicting Atrial and Ventricular Systole and Diastole

Global and Indian Burden of CVDs:

Cardiovascular diseases (CVDs) are the leading cause of mortality worldwide and a major contributor to disability. Key patterns, time trends, and disparities between India and global averages are highlighted, supported by data from sources such as the Global Burden of Disease (GBD) study, World Health Organization (WHO), Institute for Health Metrics and Evaluation (IHME), Indian national health reports, and relevant research. (Bai et al., 2023; Hu et al., 2024; R. Li et al., 2024; Pörschmann et al., 2024; Xu et al., 2024)

Table 1. Key CVD Burden Metrics: Global vs India (Comparing approximate data around 2019–2021)

Metric	Global	India
Annual CVD Deaths	~18.6 million (2019); 19.9 million (2021). CVD causes ~32% of all global deaths.	2.6–2.9 million (2017–2021). CVD causes ~26–30% of all Indian deaths.
Age-Standardized CVD Death Rate (per 100,000)	239.9 (global average, 2019). Steadily declined ~33% from ~355 in 1990.	~268–272 (India, ~2016–2021). About 1.2× higher than global rate. Modest decline or plateau in recent decade.
CVD Prevalence (cases)	523 million living with CVD (2019) globally. Up from ~300 million in early 2000s (nearly doubled since 1990).	54.5 million living with CVD (2016) in India. >2× increase from ~25.7 million in 1990. Likely >60 million by 2020s.
Annual CVD DALYs (total)	~392 million DALYs lost (2019) globally (24% increase since 2000). CVD is the #1 cause of healthy years lost worldwide.	~13.6% of India's total DALYs in 2017 were due to CVD (up from 6.9% in 1990). India contributes a large share of global CVD DALYs (e.g. ~23% of IHD DALYs).

Premature Mortality (before age 70)	~1 in 3 global CVD deaths is premature (exact global fraction ≈33%). Higher in low-income regions, lower in high-income.	~62% of CVD deaths in India are premature – a much greater premature fraction than global average. Large impact on working-age population.

CVD Burden in India: Overview and Trends (2005–2024):

Mortality: India has witnessed a dramatic rise in cardiovascular disease burden over the last two decades. CVDs are now the leading cause of death in India, accounting for an estimated 26.6% of all deaths in 2017 (up from only 15.2% of deaths in 1990)

Major Types of Cardiovascular Diseases: Global vs India (Beijian Zhang MD et al., 2024; Lv et al., 2024a; Minhas et al., 2024; Muharram et al., 2024; Reddy et al., 2021; Wilson and Poh, 2023)

Coronary Artery Disease (ischemic heart disease – IHD): This is the single largest cause of CVD deaths worldwide. Globally, IHD (which includes heart attacks, angina, etc.) was responsible for about 9.14 million deaths in 2019 – roughly half of all CVD deaths. It caused an estimated 182 million DALYs globally in 2019 , reflecting its huge impact

Stroke (Cerebrovascular Disease): Stroke (including ischemic stroke and hemorrhagic stroke) is the second-leading cause of CVD deaths globally. In 2019, there were about 6.55 million stroke deaths worldwide , accounting for roughly one-quarter of all CVD deaths.

Hypertensive Heart Disease: This refers to heart conditions caused by long-standing high blood pressure, including left ventricular hypertrophy, heart failure, etc. Globally, hypertensive heart disease (HHD) caused about 1.16 million deaths in 2019 (around 6% of CVD deaths). **Rheumatic Heart Disease (RHD):** RHD is a preventable CVD caused by rheumatic fever (streptococcal infection) damaging heart valves, typically affecting children and young adults. **Other Cardiovascular Diseases:** In addition to the above, several other cardiovascular conditions contribute to the total burden. These include cardiomyopathies and myocarditis (diseases of the heart muscle, including those due to viral infections or alcohol; globally significant but less common than IHD/HHD), atrial fibrillation and other arrhythmias, congenital heart diseases, aortic aneurysm and dissections, endocarditis, and peripheral artery disease. Collectively, these "other" CVDs make up the remaining ~10–15% of CVD DALYs globally. In 2019, for example, there were an estimated 0.37 million deaths from aortic aneurysm and ~0.34 million from atrial fibrillation/flutter worldwide (GBD 2019 data), plus additional from cardiomyopathies, etc. India, by virtue of its population size, also sees large absolute numbers of these conditions, though their share of India's CVD burden is relatively smaller compared to IHD and stroke. One notable point: heart failure as a syndrome is a major outcome of many CVDs (IHD, HHD, RHD, etc.), and its prevalence is increasing in India. An estimated 8–10 million Indians have heart failure. Many heart failure cases in India occur at

younger ages and are often due to untreated rheumatic or hypertensive heart disease, whereas in Western nations heart failure typically results from ischemic heart disease in older patients.

Additionally, India has to contend with a dual burden of continued infectious contributors to CVD (like tuberculosis causing tuberculous

pericarditis, or Chagas disease in some areas, though not as prevalent as in Latin America) alongside the usual degenerative causes.

Plant Profile:

- **Biological source**: It is leaves obatined from the plant, Grewia hirsuta Vahl
- **Family:** Malvaceae

Taxonomy:

- **Kingdom:** Plantae
- **Phylum:** Tracheophytes
- **Class:** Eudicots
- **Order:** Malvales
- **Family:** Malvaceae
- **Genus:** Grewia
- **Species:** hirsuta

Figure 3: Grewia hirsuta Vahl

Common Name:

- Bengali: Kukurbicha;
- Hindi: Kakarundah, Kukurbicha, phrongli;
- Kannada: Udipe, Dadachelu, Gandaudipe, Chikkudipe;
- Khasi: Soh synting;
- Marathi: Govli;
- Sanskrit: Gudasarkara, Nagabala;
- Tamil: Kalunnu, Tavidu, Tavadu, Ttavuttai ;
- Telugu: Chimachipuru

Distribution :

- Global Distribution : India, Bangladesh and Sri Lanka
- Indian distribution : State - Kerala, District/s: Palakkad, Idukki, Wayanad

Chemical Constituants:

Grewia hirsuta is rich in a diverse array of bioactive phytochemicals across different parts of the plant (leaves, roots, fruits, and whole plant). Prominent secondary metabolites include flavonoids (e.g., quercetin, kaempferol), phenolic compounds (e.g., gallic acid, caffeic acid), tannins, alkaloids, saponins, glycosides, coumarins, steroids, terpenoids, and reducing sugars.

Morphology and Occurrence :

Nagbala Crossberry is a shrub or small trees, with branchlets coarsely gray-brown hairy. Leaf stalks are 2-3 mm long, tomentose. Leaves are lance-shaped, 6-14 cm long, 2-3.5 cm wide, leathery, black-brown when dried, velvety. Lateral basal veins are up to 1/2 as long as leaf blade, lateral veins 4-5 pairs, base narrow, shallowly hreat-shaped, margin toothed, tip long pointed or rarely blunt.

MATERIAL AND METHOD:

Experimental animals - Male Wistar rats (200–250 g)

Chemicals:

Lyophilized doxorubicin powder was obtained from Khandelwal Laboratories Pvt. Ltd., India. Creatine kinase-MB (CK-MB) and lactate dehydrogenase (LDH) assay kits were procured from Aspen Laboratories, Delhi, India. The serum glutamic-oxaloacetic transaminase (SGOT) kit was sourced from ERBA Diagnostics, Germany.

Key reagents including Nitro Blue Tetrazolium (NBT), 5,5′-Dithiobis(2-nitrobenzoic acid) (DTNB), and Triton X-100 were purchased from HiMedia Laboratories, Mumbai, India. Phosphoric acid, sodium carbonate, EDTA, and dipotassium hydrogen phosphate were acquired from Loba Chemie, Mumbai, India, while monopotassium dihydrogen phosphate, n-butanol, potassium chloride (KCl), and thiobarbituric acid (TBA) were supplied by Sigma Aldrich, Germany. Additional chemicals such as formaldehyde, hydrogen peroxide, and sodium chloride (NaCl) were obtained from Rankem, India. Hydroxylamine hydrochloride was supplied by Titan Biotech; the Grease reagent was purchased from Fluka Analytical, Switzerland; and ELISA kits for TNF-α and IL-1β were procured from eBioscience, San Diego, USA.

Plastic and glass wares:

Eppendorf tubes (2 ml), test tubes, conical flask (250 ml), beakers (50ml,100ml, 250ml), measuring cylinders (10ml, 50ml), Petri dish, pipette (1ml, 2ml,5ml), etc.

Equipment:

The experimental procedures utilized a PowerLab data acquisition system (AD Instruments, Australia) and a homogenizer (Model RQ127A, Remi Motors Ltd., India). A cooling centrifuge (Model C30BL, Remi, India) and a vortex mixer (Genei) were employed for sample processing. Microscopic evaluations were performed using an inverted microscope (Motic AE31) equipped with an MXH-100 camera, and tissue sectioning was carried out using a microtome (Leica RM 2125, Germany). Additional equipment included a precision weighing balance (Precisa 205 A SCS), eight-channel micropipette (Lobalife), 12-channel micropipette (Borosil), and single-channel micropipettes of varying volumes (2, 20, 200, and 1000 µL) from TARSONS. Pipette tips were sourced from HiMedia, while 96-well microplates (Nunc, Denmark) were used for assay procedures. A microplate reader (Biotek), deep freezer (Blue Star), UV-visible spectrophotometer (Shimadzu UV-1201, Japan), heating mantle, and additional vortex mixer (Genei) were also part of the laboratory instrumentation.

Collection and authentication of plant Material:

Leaves of Grewia hirsuta Vahl were collected in July 2024 from the Markhanda forest region, located in Gadchiroli District, Maharashtra, India. The plant material was authenticated by a qualified botanist at Sandip University, Nashik, India. A corresponding herbarium specimen was prepared and deposited at the same institution under voucher number SUN2024/07/08.

Extraction :

A total of 1000 g of dried leaf powder was extracted by maceration in a hydroalcoholic solvent system (70:30 v/v) with intermittent stirring at 25 ± 2°C for three days. The mixture was then filtered through a sterile cotton plug using a Buchner funnel. The filtrate was concentrated under reduced pressure using a rotary evaporator, resulting in 37.21 g of crude hydroalcoholic extract. This extract was subsequently used for the assessment of cardioprotective activity. The percentage yield of the extract was calculated using the following formula:

Percentage yield= Weight of Extract / Weight of powdered drug ×100

Pharmacological Investigation:

Drugs/Chemicals : Doxorubicin

Quarantine and Acclimatization :

Quarantine entails the isolation of newly procured animals from the resident colony to evaluate their health condition and potential microbial burden. In the present study, newly acquired Wistar albino rats were quarantined for a period of one week to minimize the risk of pathogen transmission to the established stock and to allow for physiological and nutritional stabilization before their inclusion in experimental procedures.

Housing:

The animals were housed in a well-ventilated facility under controlled environmental conditions, with temperature and relative humidity maintained within the range of 55–65%. They were kept in spacious polypropylene cages lined with paddy husk, which served as bedding material.

Diet and Water:

Animals were supplied with a standard pellet diet and purified water, both available ad libitum except during specified fasting periods. Bedding was changed regularly to ensure hygienic housing conditions throughout the study.

Drug Administration:

Drugs were administered orally using a feeding tube attached to a syringe, allowing for precise and consistent dose delivery. The dosage for each animal was determined in accordance with the experimental protocol.

Preparation of Dose:

The hydroalcoholic extract of Grewia hirsuta was evaluated at oral dose levels of 50, 100, and 150 mg/kg. Each dose was prepared by precisely weighing the required amount of extract and suspending it in a 0.3% carboxymethyl cellulose (CMC) solution formulated in distilled water.

Drug Administration:

Drugs were administered orally through oral gavage. An oral feeding tube fixed to a syringe needle was used for precise dosage delivery. The drug quantity was administered as required.

Experimental procedure: Doxorubicin induced Cardiotoxicity:

Male Wistar albino rats (200-250 gm.12-14 weeks ago) were randomly allocated based on serum CKMB &LDH levels in 6 groups, with n=6 animals in each group, as follows: Group I Normal Control (NC), Group II Model Control (MC), Group III GH 50 mg/kg, Group IV GH 100 mg/kg, Group V GH 150 mg/kg, and Group VI received only GH extract (150 mg/kg), Cardiotoxicity was induced by administration of doses of Doxorubicin (30 mg/kg, i.p.) on Following days 1,7,14,21,28. Group I received Drinking Water (p.o), and Group II was given Doxorubicin (3 mg/kg i.p.) alone for 1, 7,14,21,28 days. Along with doxorubicin, and Groups III-V was given test drug GH 50 mg/kg p.o, 100 mg/kg p.o, 150 mg/kg p.o, respectively for 28 days.

Table 2 : Distribution of Experimental animals

Groups	Treatment	No of animals	Route
Group 1	Control group	6	Orally
Group 2	Model Control group	6	Orally
Group 3	Lower dose of Grewia hirsuta extract (50 mg/kg) + Dox	6	Orally
Group 4	Moderate dose of Grewia hirsuta extract (100 mg/kg) + Dox	6	Orally
Group 5	Higher dose of Grewia hirsuta	6	Orally

	extract (150 mg/kg) + Dox		
Group 6	Grewia hirsuta extract (PERSE) (150 mg/kg)	6	Orally

Collection of Biological sample: Blood and Serum:

At the end of the 28-day treatment period, blood samples were collected via the retro-orbital plexus under anesthesia. Animals were subsequently sacrificed using phenobarbital anesthesia. The collected blood was centrifuged at 3000 rpm for 15 minutes using a centrifuge (Plasto Craft Industries Pvt. Ltd, R4R-V/FA) to separate the serum, which was then subjected to biochemical analysis.

Experimental animals: Male Wistar rats (200-250 g)

The animals were divided into six experimental groups for evaluation of the effect of extract. A total of 36 animals were used for this study. Each group consisted of 6 rats.

Control Group (Group 1):

✓ This group received a placebo or vehicle (no extract) to serve as the baseline or control for comparison.

Doxorubicin-Induced Cardiotoxicity Group (Group 2):

✓ Rats in this group were administered doxorubicin to induce cardiotoxicity. They did not receive extract.

Doxorubicin + Low-Dose GH Group (Group 3):

✓ Rats in this group were administered doxorubicin to induce cardiotoxicity and received a low dose of extract for evaluation of its potential cardioprotective effects.

Doxorubicin + Moderate-Dose GH Group (Group 4):

✓ Rats in this group were administered doxorubicin to induce cardiotoxicity and received a moderate dose of extract to assess its impact on cardioprotection.

Doxorubicin + High-Dose GH Group (Group 5):

✓ Rats in this group were administered doxorubicin to induce cardiotoxicity and received a high dose of extract to determine the potential dose-dependent effects on cardioprotection.

GH-Treatment Group (Group 6):

✓ Rats in this group were treated with GH alone, without exposure to doxorubicin. This group served to assess the effects of GH in the absence of doxorubicin-induced cardiotoxicity.

Upon completion of the final treatment day, the rats were euthanized. Electrocardiographic and hemodynamic parameters were recorded, followed by blood collection. Heart tissues were excised and processed for biochemical, antioxidant, and cytokine analyses, as well as for histopathological evaluation.

Electrocardiography :

Rats were anesthetized using urethane and secured in a supine position on a surgical board. Electrocardiograms (ECG) were recorded by inserting three needle electrodes subcutaneously. The positive and negative electrodes were placed on the left and right forelimbs, respectively, oriented toward the heart, while the neutral electrode was positioned on the hind limb. These electrodes were connected to the PowerLab data

acquisition system (AD Instruments, Australia) for ECG recording. (Reddy et al., 2015)

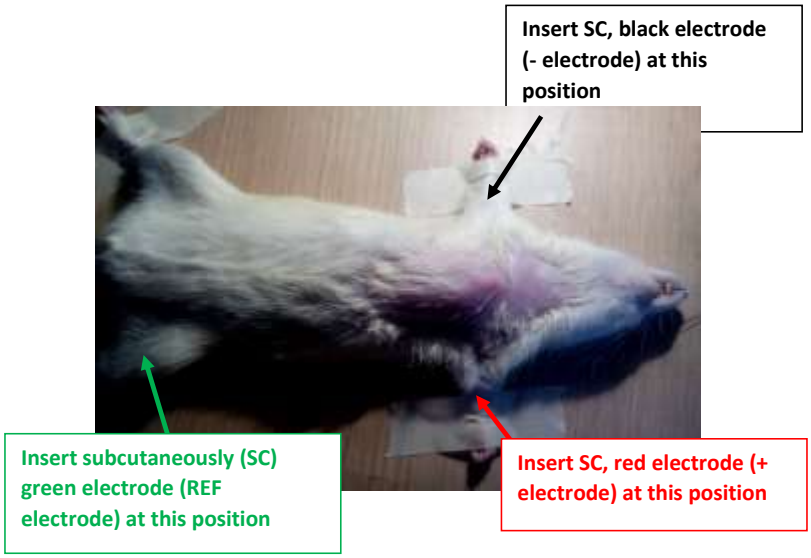

Figure 4: ECG electrode positioning

Hemodynamic parameter:

Following administration of urethane (1.25 g/kg, i.p.) and atropine sulfate (0.05 mg/kg, i.p.) to reduce bronchial secretions during surgery, ECG recordings were obtained from anesthetized rats. The animals were secured in a supine position using adhesive strips to immobilize the limbs. Core body temperature was continuously monitored via a rectal probe connected to the PowerLab data acquisition system (AD Instruments, Australia) and maintained at approximately 37°C using a mercury lamp.

A midline ventral incision was made in the neck to perform a tracheotomy. The trachea was incised and cannulated with a polyethylene tube (P50). The left jugular vein was cannulated using a polyethylene tube (P10) for continuous saline infusion to maintain fluid balance. The right carotid artery was carefully isolated and cannulated with a polyethylene tube (P30), connected to a three-way cannula prefilled with heparinized saline. This setup was linked to the PowerLab system via a pressure transducer to record systolic arterial pressure (SAP), diastolic arterial pressure (DAP), mean arterial pressure (MAP), and heart rate.

After recording hemodynamic parameters, animals were euthanized using an intravenous overdose of pentobarbital sodium (100 mg/kg). Blood samples were collected, and hearts were excised for biochemical, immunohistochemical, and western blot analyses. Tissues designated for biochemical and protein analysis were snap-frozen in liquid nitrogen, while samples intended for histological examination were fixed in 10% buffered formalin. (Reddy et al., 2015)

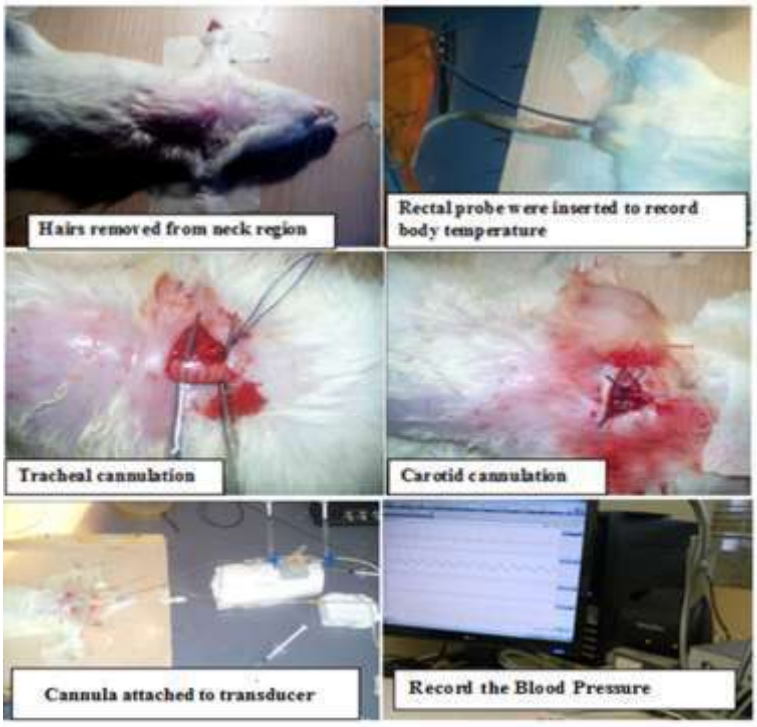

Figure 5: Surgical procedure for recording hemodynamic parameters

Biochemical parameter:

Figure 6 : Microplate reader

Preparation of homogenate:

Frozen heart tissues were retrieved from liquid nitrogen, accurately weighed, and homogenized to prepare a 10% (w/v) myocardial tissue suspension in phosphate buffer (pH 7.4) under cold conditions. The homogenate was then centrifuged at 7000 rpm for 20 minutes using a high-speed centrifuge. The resulting supernatant was collected and used for the assessment of various biochemical parameters.

❖ **Tissue parameter**:

- **Estimation of creatine kinase-MB (CK-MB):**

CK-MB isoenzyme was estimated in homogenate using commercial kit Mfd. Aspen Laboratories, Delhi (India).

Principle:

The sample was incubated in CK-MB reagent, which includes the anti-CK-M antibody. The activity of the non-inhibited CK-B is then determined using the following series of reactions:

$$\text{ADP + Creatine Phosphate} \xrightarrow[\text{CK}]{} \text{Creatinine + ATP}$$

$$\text{ATP + Glucose} \xrightarrow{\text{HK}} \text{ADP + Glucose -6-Phosphate}$$

$$\text{Glucose -6-Phosphate + NAD}^{+} \xrightarrow{\text{G6PDH}} \text{6-Phosphogluconate + NADH +H}^{+}$$

Creatine kinase-B (CK-B) catalyzes the reversible transfer of a phosphate group from creatine phosphate to ADP, yielding ATP and creatine. In this coupled enzymatic assay, hexokinase (HK) acts as an auxiliary enzyme, utilizing the generated ATP to phosphorylate glucose, forming glucose-6-phosphate and ADP. Subsequently, glucose-6-phosphate is oxidized to 6-phosphogluconate, a reaction that simultaneously generates NADH. The rate of NADH formation, monitored spectrophotometrically at 340 nm, is directly proportional to CK-B activity in the serum.

Procedure:

A volume of 1000 µL of reagent was pipetted into a reaction tube, followed by the addition of 50 µL of the serum sample. The mixture was thoroughly mixed and incubated at 37°C. Absorbance readings were taken at three 1-minute intervals. The mean change in absorbance per minute (ΔA/min) was calculated, and enzyme activity was determined by multiplying ΔA/min by the factor 3376.

- **Lactate dehydrogenase (LDH) isoenzyme:**

LDH was estimated in homogenate using a commercial kit from span Mfd. Aspen Laboratories, Delhi (India).

Principle:

Lactate dehydrogenase (LDH) catalyzes the oxidation of lactate to pyruvate in the presence of NAD^{+}, which is concurrently reduced to NADH. The rate of NADH generation, monitored spectrophotometrically at 340 nm, is directly proportional to the activity of LDH-L in the serum.

$$\text{Pyruvate + NADH} \xrightarrow[\text{LDH}]{} \text{Lactate + NAD}$$

Procedure:

A total of 1000 µL of reagent was pipetted into the reaction vessel, followed by the addition of 50 µL of the serum sample. The mixture was thoroughly mixed and incubated at 37°C. Absorbance was measured initially and then at three successive 1-minute intervals. The average change in absorbance per minute (ΔA/min) was calculated, and the enzyme activity was determined by multiplying ΔA/min by the factor 3376.

Preparation of serum

Blood samples were collected into plain tubes and allowed to clot at room temperature. Subsequently, the serum was separated by centrifugation at 4000 rpm for 15 minutes at 4 °C.

❖ **Serum parameter:**

- **Estimation of SGOT:**

SGOT estimated in serum using a commercially available kit (ERBA diagnostic Mannheim, Germany)

Principle:

SGOT (AST) catalyzes the transfer of an amino group from L-aspartate to α-ketoglutarate, resulting in the formation of oxaloacetate and glutamate. The generated oxaloacetate then reacts with NADH in the presence of malate dehydrogenase, producing NAD^+. The rate of NADH oxidation, observed as a decrease in absorbance, is directly proportional to the SGOT (AST) activity in the sample.

Procedure:

A volume of 1000 µL of reagent was pipetted into the reaction tube, followed by the addition of 100 µL of the serum sample. The mixture was gently mixed and incubated at 37°C. Absorbance was recorded initially and at three subsequent 1-minute intervals. The mean change in absorbance per minute (ΔA/min) was calculated, and SGOT (AST) activity was determined by multiplying ΔA/min by the factor 1768.

❖ **Antioxidant parameters:**

- **Tissue parameter**

- **Estimation of total protein content:**

The protein content in cardiac tissue homogenate was quantified using the Bradford method (Bradford et al., 1976), employing bovine serum albumin as the standard. The protein reagent was prepared by dissolving 100 mg of Coomassie Brilliant Blue G-250 in 50 mL of 95% ethanol, followed by the addition of 100 mL of 85% (w/v) phosphoric acid. The resulting mixture was diluted with distilled water to a final volume of 1 liter, yielding a reagent containing 0.01% (w/v) Coomassie Brilliant Blue G-250, 4.7% (w/v) ethanol, and 8.5% (w/v) phosphoric acid.

Aliquots containing 10–100 µg of protein were transferred into 12 × 100 mm test tubes, with the volume adjusted to 0.1 mL using an appropriate buffer. Each tube received 5 mL of the prepared protein reagent, and the contents were mixed thoroughly either by inversion or vortexing. After 2 minutes, the absorbance was measured at 595 nm against a reagent blank. Total protein content was expressed in milligrams per gram of tissue.

- **Estimation of lipid peroxidation** :

Malondialdehyde (MDA) is a naturally occurring byproduct generated during lipid peroxidation, and it can also arise from prostaglandin biosynthesis within cells. MDA readily reacts with amino groups on proteins and other biomolecules, forming a variety of adducts. These adducts are also capable of interacting with DNA bases, contributing to mutagenic effects and potentially promoting carcinogenesis. Elevated levels of lipid peroxidation products, as indicated by increased MDA concentrations, have been associated with numerous pathological conditions and disease states.

Principle :

MDA, a secondary product of lipid peroxidation, reacts with thiobarbituric acid (TBA) to form a red-colored chromogen. This pigment is subsequently extracted using an n-butanol–pyridine mixture and quantified by measuring its absorbance at 532 nm.

Procedure:

Malondialdehyde (MDA) levels were quantified using the thiobarbituric acid reactive substances (TBARS) assay as described by Ohkawa et al. (1979). The standard used for calibration was 1,1,3,3-tetraethoxypropane (Sigma Chemicals, USA). Results were expressed in micrograms of MDA per milligram of protein (µg/mg protein).

Briefly, 100 µL of tissue homogenate was mixed with 600 µL of 1% orthophosphoric acid (pH 3.5)

and 100 µL of 0.6% thiobarbituric acid. The mixture was incubated at 95 °C for 60 minutes, followed by rapid cooling in an ice bath. After cooling, 1.0 mL of distilled water and 1.0 mL of n-butanol were added, and the mixture was vortexed thoroughly. The reaction mixture was then centrifuged at 5000 rpm for 20 minutes. The intensity of the pink chromogen in the organic (butanol) layer was measured spectrophotometrically at 532 nm to determine MDA content.

- **Estimation of Catalase (CAT):**

Catalase is a widely distributed antioxidant enzyme present in both mammalian and non-mammalian cells. Its principal role is the dismutation of hydrogen peroxide into water and molecular oxygen, thereby mitigating oxidative damage. In eukaryotes, catalase is a heme-containing enzyme found in high concentrations in the liver, kidney, and erythrocytes, with comparatively lower levels in connective tissues. The enzyme is primarily localized within the peroxisomes, a key subcellular organelle involved in reactive oxygen species detoxification.

Principle:

Catalase catalyzes the decomposition of hydrogen peroxide (H_2O_2) into water and oxygen. The rate at which hydrogen peroxide is broken down is directly proportional to the concentration of catalase present in the sample.

Procedure:

Catalase activity, an indicator of endogenous antioxidant capacity, was assessed following the method described by Goth et al. (1991). Results were expressed as micrograms of catalase per milligram of protein (µg/mg protein). The assay mixture consisted of 1.0 mL of 50 mM phosphate buffer (pH 7.0), 0.1 mL of 30 mM hydrogen peroxide, and 50 µL of tissue supernatant. The decomposition of hydrogen peroxide was monitored by measuring the decline in absorbance at 240 nm using a UV spectrophotometer, with readings taken every 30 seconds over a total duration of 260 seconds.

- **Estimation of reduced glutathione (GSH):**

Glutathione (GSH) functions as a key antioxidant across a wide range of organisms, including plants, mammals, fungi, and specific bacteria and archaea. It plays an essential role in safeguarding vital cellular components against damage induced by reactive oxygen species (ROS), such as free radicals, peroxides, lipid peroxides, and heavy metals. Structurally, GSH is a tripeptide composed of glutamate, cysteine, and glycine. It features an unusual gamma-peptide linkage between the γ-carboxyl group of glutamate and the amino group of cysteine, while cysteine is linked to glycine via a conventional peptide bond.

Principle:

Glutathione reductase (GR) plays an essential, albeit indirect, role in cellular defense against oxidative stress by maintaining adequate intracellular levels of reduced glutathione (GSH). GSH, in concert with the enzyme glutathione peroxidase (GPx), serves as a key reducing agent that detoxifies hydrogen peroxide and helps sustain redox homeostasis within the cell.

Procedure:

Myocardial glutathione (GSH) levels were estimated using the method described by Maron et al. (1979). GSH concentrations were determined by referencing a standard curve generated from commercially available GSH standards, and values

were expressed as micrograms per milligram of protein in wet tissue.

Briefly, 100 µL of tissue homogenate was mixed with 100 µL of 10% trichloroacetic acid and vortexed thoroughly. The mixture was then centrifuged at 5000 rpm for 10 minutes. From the resulting supernatant, 0.05 mL was added to a reaction mixture containing 3.0 mL of 0.3 M phosphate buffer (pH 8.4) and 0.5 mL of DTNB reagent. Absorbance was measured at 412 nm using a spectrophotometer within 10 minutes of reaction initiation.

- **Estimation of superoxide dismutase (SOD):**

Principle:

The superoxide dismutase (SOD) activity assay is based on the enzyme's ability to inhibit the reduction of nitroblue tetrazolium (NBT). In this method, superoxide anions ($O_2^{\bullet -}$) are generated via the xanthine–xanthine oxidase system, and their presence is indicated by the reduction of NBT to a blue-colored formazan. The formation of formazan is monitored spectrophotometrically at 560 nm. One unit of SOD activity is defined as the amount of enzyme required to inhibit the NBT reduction by 50% under the assay conditions.

Procedure:

Superoxide dismutase (SOD) activity was assessed following the method described by Mishra and Fridovich (1978). The assay mixture consisted of 25 µL of tissue supernatant, 100 µL of 500 mM sodium carbonate (Na_2CO_3), 100 µL of 1 mM EDTA, 100 µL of 240 µM nitroblue tetrazolium (NBT), 640 µL of distilled water, 10 µL of 0.3% Triton X-100, and 25 µL of 10 mM hydroxylamine. The reaction was monitored spectrophotometrically in kinetic mode at 560 nm, with absorbance readings recorded every minute for a total of three minutes. SOD activity was calculated and expressed as micrograms per milligram of protein.

- **Nitric Oxide Estimation (Grease reagent method):**

Principle:

The nitrite reacts with the Griess reagent and produces nitric oxide. It is an indicator of the amount of nitrite present in tissue homogenate.

Reagent:

Griess reagent

1:1 solution of 1% sulphanilamide in 5% phosphoric acid and 0.1% napthalamine dihydrochloric acid in water.

Preparation of 100ug solution:

1 ml (1000 ug) of sodium nitrite diluted with 10 ml distilled water. Dilution of sodium nitrite was prepared as 1 µg, 2 µg, 3 µg, 4 µg, 5 µg. Each test tube contained 0.1 ml, 0.2 ml, 0.3ml, 0.4ml, 0.5ml solution of 100 µg and then diluted up to 10 ml with water, respectively.

Procedure for standard curve:

Ninety-six well microplates were used for the assay. A volume of 100 µL of the sample was added to each well according to the experimental layout. Subsequently, 100 µL of Grease reagent was added to each corresponding well. A visible color change (pink or purple) was observed, indicating a positive reaction. The absorbance was then measured at 540 nm using a microplate reader to perform the colorimetric assay. (Baryan et al., 2007)

- **Cytokine's estimation of TNF-α and IL- 1β:**

A commercial ELISA kit assayed the production of TNF-α and IL-1β in the tissue supernatants. Using mouse TNF-α and IL-1β kit (eBioscience USA) according to the manufacturer's instructions.

Principle:

This assay is based on the quantitative sandwich enzyme-linked immunosorbent assay (ELISA) technique. Microplate wells were pre-coated with a monoclonal antibody specific to rat IL-1β. Standards, controls, and tissue homogenate samples were added to the wells, allowing IL-1β present in the samples to bind to the immobilized capture antibody. After washing to remove unbound substances, a polyclonal antibody conjugated to an enzyme and specific for IL-1β was added, followed by a substrate solution. The enzymatic reaction generated a blue-colored product, which changed in intensity upon the addition of a stop solution. The resulting color intensity was measured using an ELISA reader and was directly proportional to the concentration of rat IL-1β captured in the assay.

Procedure:

The ELISA plate was initially coated with 100 µL per well of capture antibody diluted in 1X Coating Buffer. After overnight incubation at 2–8°C, the plate was washed using the designated washing buffer. A 1X ELISA/ELISPOT Diluent was prepared by mixing 1 part of the 5X concentrate with 4 parts of deionized water. Each well was blocked by adding 200 µL of this 1X diluent to prevent nonspecific binding.

Following a 1-hour incubation of the tissue supernatant at room temperature, the samples were appropriately diluted, and 100 µL was added to each well. The plate was sealed and incubated at ambient temperature for 2 hours. After washing to remove unbound materials, detection antibodies were added and allowed to react for 2 hours at room temperature. Subsequently, wells were washed, and 100 µL of Avidin-HRP conjugate diluted in 1X ELISA/ELISPOT Diluent was added to each well and incubated for 30 minutes at room temperature.

After thorough washing, 100 µL of TMB (tetramethylbenzidine) substrate solution was added to each well and the plate was incubated for 15 minutes at room temperature. The reaction was terminated by adding 50 µL of stop solution (2 M sulfuric acid) to each well.

- **Histological examination:**

Principle:

Histopathology involves the microscopic examination of biopsy or surgically excised tissue samples to identify pathological changes indicative of disease. The tissue sections are processed, mounted on glass slides, and stained with one or more dyes to enhance the visualization of cellular structures under the microscope. Staining highlights specific cellular components, while counterstains are used to improve overall contrast. Hematoxylin and Eosin (H&E) staining remains the gold standard in histopathological evaluation. Hematoxylin stains cell nuclei blue, whereas eosin stains the cytoplasm and connective tissues various shades of pink, providing clear morphological detail for diagnostic interpretation.

Procedure:

Rat hearts were excised, promptly rinsed with saline solution, and fixed in 10% buffered formalin. The fixed tissues were subsequently embedded in paraffin, and 3 µm thick sections were obtained using a microtome (Leica RM 2125, Germany). The tissue sections were stained with

hematoxylin and eosin (H&E), sourced from Sigma Aldrich. Microscopic evaluation was performed using a light microscope, and representative images were captured. Image analysis was conducted using ImageJ software to document and evaluate histological features.

Statistical analysis:

The obtained results were reported in mean ± SEM for each group. Statistical analysis was performed by one-way analysis of variance (ANOVA) followed by Bonferroni post hoc test using a graph pad, prism software, version 10.1, USA.

NETWORK PHARMACOLOGY :

Screening active phytoconstituents Grewia hirsuta Vahl leaves :

The identification of bioactive phytoconstituents present in Grewia hirsuta Vahl leaves was carried out through an extensive review of scientific literature and phytochemical databases. Key constituents were primarily retrieved from the Indian Medicinal Plants, Phytochemistry, and Therapeutics (IMPPAT) database (https://cb.imsc.res.in/imppat/). Additional relevant data were compiled from peer-reviewed publications and reports available on platforms such as Google Scholar, PubMed, and ScienceDirect.

Retrieving phytoconstituents-associated targets:

The canonical SMILES of all identified phytoconstituents were retrieved from the PubChem database (https://pubchem.ncbi.nlm.nih.gov/). Target prediction for each compound was performed by inputting the canonical SMILES into six distinct target prediction platforms, with a similarity threshold set at 0.5. The databases utilized for this analysis included SwissTargetPrediction (http://www.swisstargetprediction.ch/), Similarity Ensemble Approach (SEA) (https://sea.bkslab.org/), BindingDB (https://www.bindingdb.org/rwd/bind/chemsearch/marvin/FMCT.jsp), PASS Online (https://www.way2drug.com/passtargets/), ChEMBL (https://www.ebi.ac.uk/chembl/), and SuperPred Target Prediction (https://prediction.charite.de/subpages/target_prediction.php).

Retrieving disease-associated targets

Genes associated with cardiotoxicity and cardiac diseases were identified using keyword-based searches in established biomedical databases. Gene information was retrieved from DisGeNET (https://disgenet.com/), GeneCards (https://www.genecards.org/home), and MalaCards (https://www.malacards.org/). The corresponding UniProt identifiers for the selected genes were obtained using the UniProt ID Mapping tool (https://www.uniprot.org/id-mapping) to ensure standardized protein annotation for subsequent analyses.

Constructing network and analysing :

Overlapping targets between the predicted phytoconstituent-associated proteins and disease-related genes were identified using the Venny tool (https://bioinfogp.cnb.csic.es/tools/venny/). Protein–compound interaction networks were subsequently constructed using the STRING database (https://string-db.org/) to investigate potential functional associations. Further network analysis was performed in Cytoscape (version 3.10.3), where the CytoHubba plugin was utilized to assess network centrality through degree-based and other topological ranking algorithms.

Pathway Enrichment Analysis :

Gene Ontology (GO) and KEGG pathway enrichment analyses were conducted for the top 20 target nodes using the DAVID platform. GO analysis was employed to identify the associated biological processes, cellular components, and molecular functions. In parallel, KEGG pathway analysis offered insights into the key signaling pathways involved, using annotations sourced from the KEGG database (https://www.genome.jp/kegg/pathway.html).

Molecular docking experiment :

Computational molecular docking studies were performed on a Windows 10 platform equipped with an Intel® Core™ i7-8700 CPU @ 3.20 GHz and 16 GB RAM, utilizing the Schrödinger Suite 2019-1 through Maestro 11.9 (Schrödinger, LLC, NY, 2019). The interaction patterns and potential binding affinities between the selected phytoconstituents and core target proteins were evaluated using the molecular docking module within the Maestro interface.

a) Ligand and protein preparation

All ligand structures were constructed using the Maestro Build Panel and prepared using the LigPrep module in the Schrödinger Suite. LigPrep generated low-energy three-dimensional conformers and optimized molecular geometries using the MMFF94s force field while preserving defined chiral centers. Core protein targets were retrieved from the RCSB Protein Data Bank (https://www.rcsb.org/) based on corresponding gene sequences. Selection criteria included a resolution of ≤ 2.5 Å, Homo sapiens origin, and determination via X-ray crystallography. Protein structures were downloaded in PDB format and processed using the Protein Preparation Wizard in Maestro. This workflow involved removal of water molecules, optimization of hydrogen bonding, and energy minimization to obtain stable, low-energy conformations suitable for molecular docking.

b) Identification of active site

The SiteMap tool was utilized to predict potential binding sites on the prepared protein structure by identifying regions likely to accommodate active ligands. Among the detected sites, the one with the highest druggability score (D-score closest to 1) was selected as the active site for grid generation in the molecular docking process.

c) Molecular docking

The prepared ligands and protein targets were docked using the Glide module within the Schrödinger Suite, employing the Glide Ligand Docking protocol in Extra Precision (XP) mode. Docking was conducted at the active sites identified by the SiteMap tool, with ligand flexibility taken into account to enhance binding accuracy and predict optimal interaction conformations.

RESULT:

Collection and authentication of plant Material:

Leaves of *Grewia hirsuta* Vahl were collected in July 2024 from the Markhanda forest region, located in Gadchiroli District, Maharashtra, India. The plant material was authenticated by a qualified botanist at Sandip University, Nashik, India. A corresponding herbarium specimen was prepared and deposited at the same institution under voucher number SUN2024/07/08.

Extraction:

A total of 1000 g of dried leaf powder was extracted by maceration in a hydroalcoholic solvent system (70:30 v/v) with intermittent

stirring at 25 ± 2°C for three days. The mixture was then filtered through a sterile cotton plug using a Buchner funnel. The filtrate was concentrated under reduced pressure using a rotary evaporator, resulting in 37.21 g of crude hydroalcoholic extract. This extract was subsequently used for the assessment of cardioprotective activity.

Yield of Extract – 3.7 %

PHARMACOLOGİCAL EVALUATİON:

Electrocardiographic parameter:

The effect of *Grewia hirsuta* leaves hydroalcoholic extract on cardiac electrophysiology in doxorubicin induced cardiotoxicty are summarized.

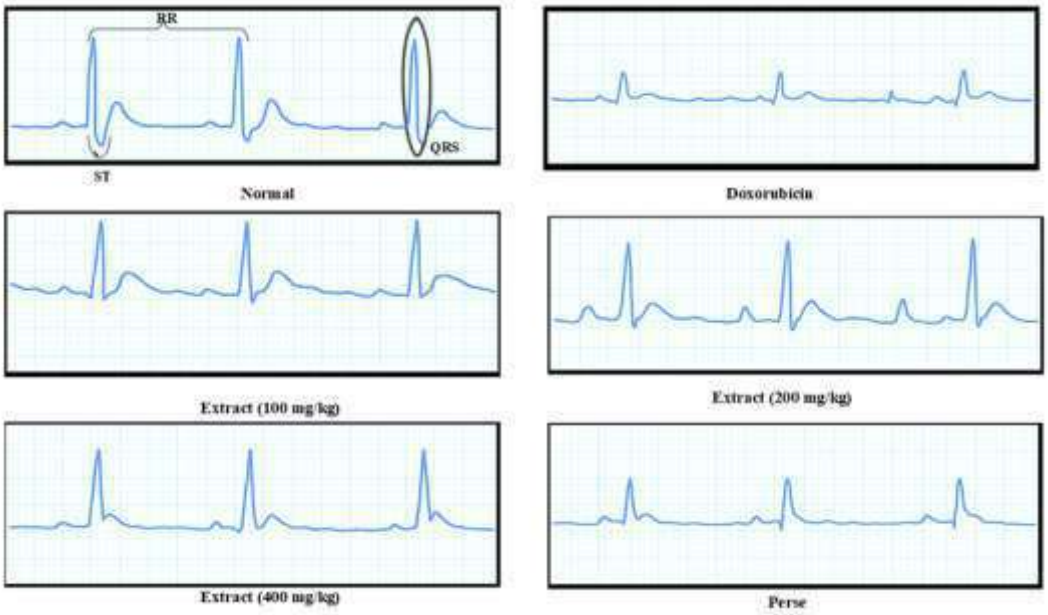

Figure 7: Photograph showing the changes in the rat ECG wave front

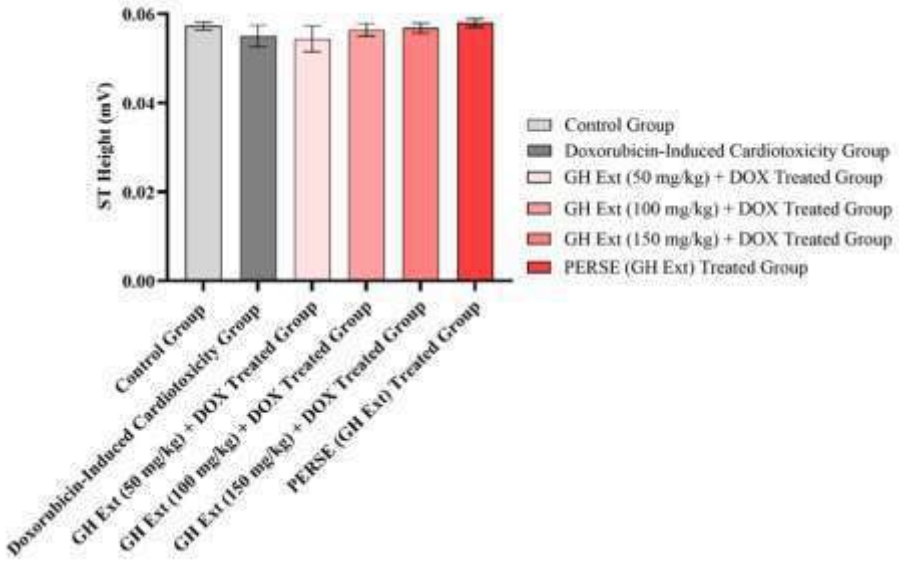

Figure 8: Effect of GHE on changes in ST height

Data was expressed as the mean ± SEM (n=6).

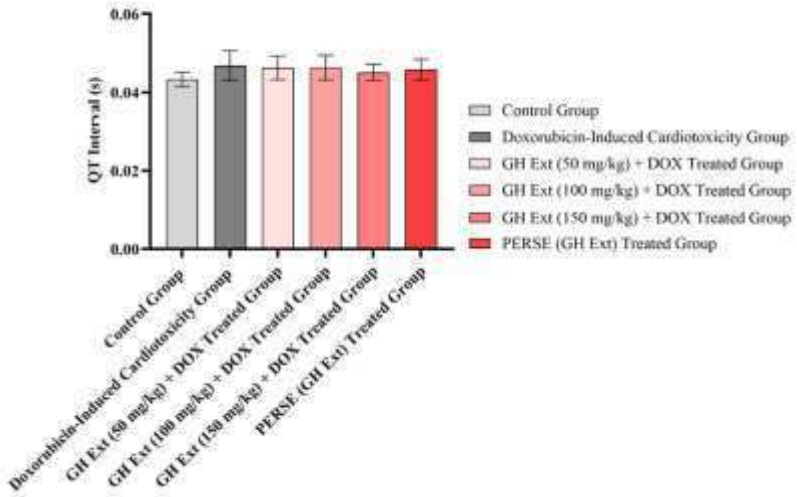

Figure 9: Effect of GHE on changes in QT interval

Data was expressed as the mean ± SEM (n=6).

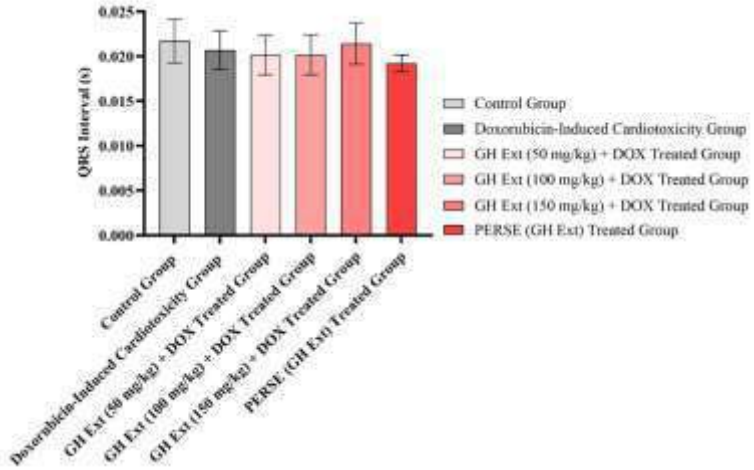

Figure 10: Effect of GHE on changes in QRS interval

Data was expressed as the mean ± SEM (n=6).

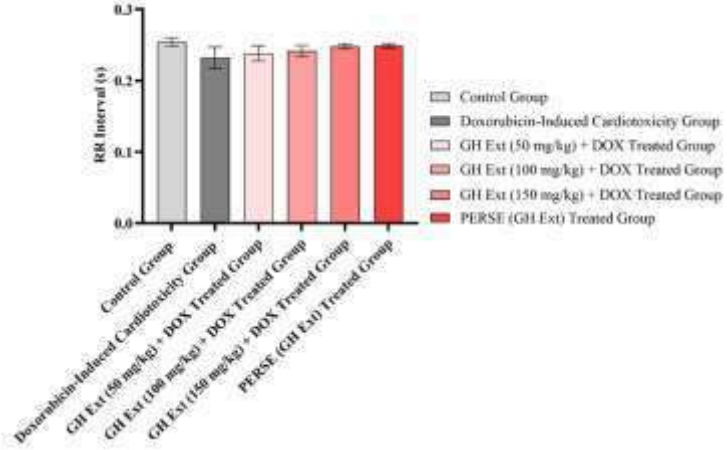

Figure 11: Effect of GHE on changes in RR interval

Data was expressed as the mean ± SEM (n=6).

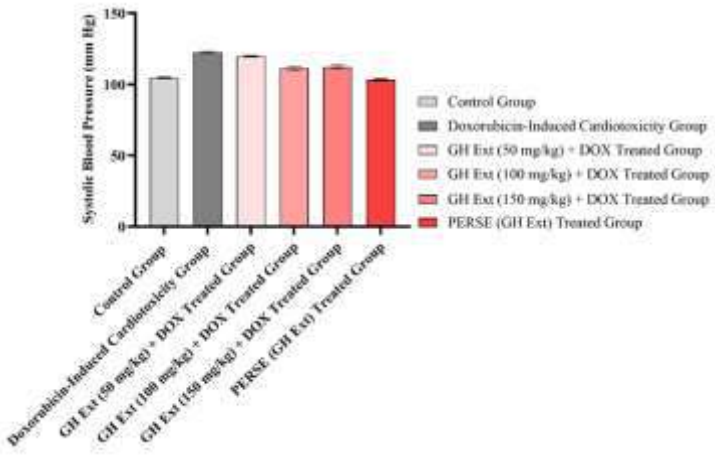

Figure 12: Effect of GHE on changes in systolic blood pressure

Data was expressed as the mean ± SEM (n=6).

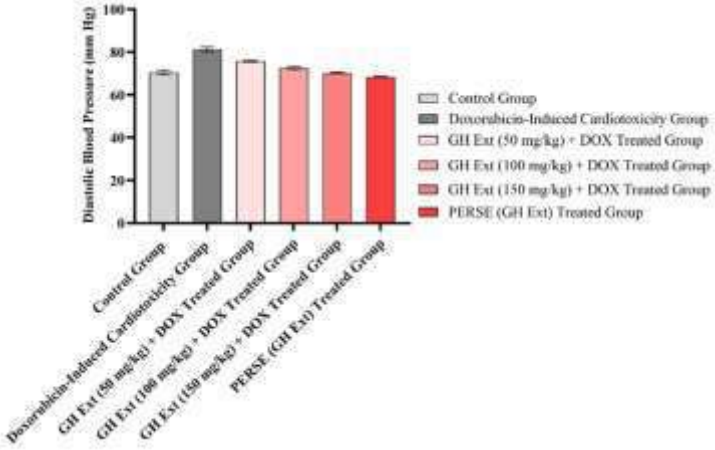

Figure 13: Effect of GHE on changes in diastolic blood pressure

Data was expressed as the mean ± SEM (n=6).

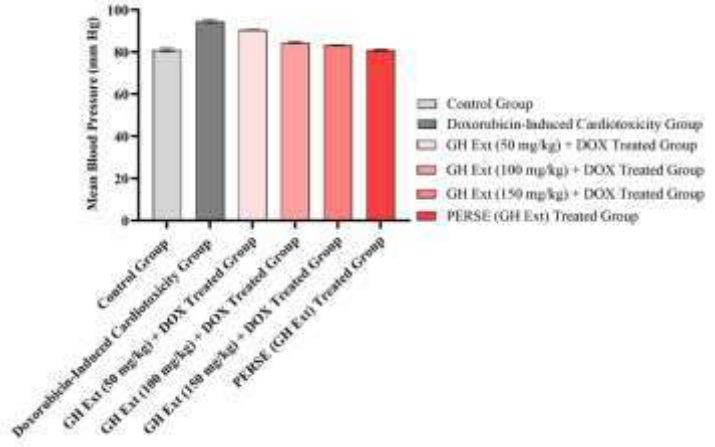

Figure 14: Effect of GHE on changes in mean blood pressure

Data was expressed as the mean ± SEM (n=6).

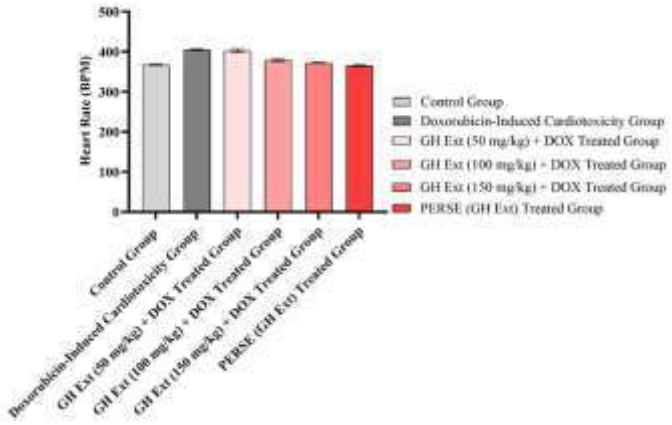

Figure 15: Effect of GHE on changes in heart rate

Data was expressed as the mean ± SEM (n=6).

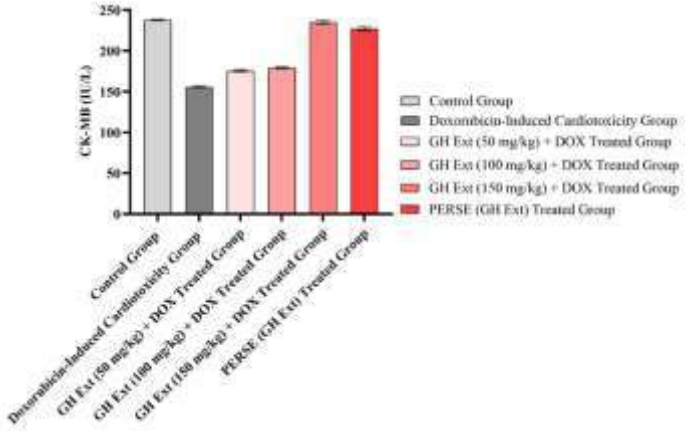

Figure 16: Effect of GHE on changes in CK-MB

Data was expressed as the mean ± SEM (n=6).

Effect of GHE on changes in SOD in doxorubicin induced cardiotoxicity in rats

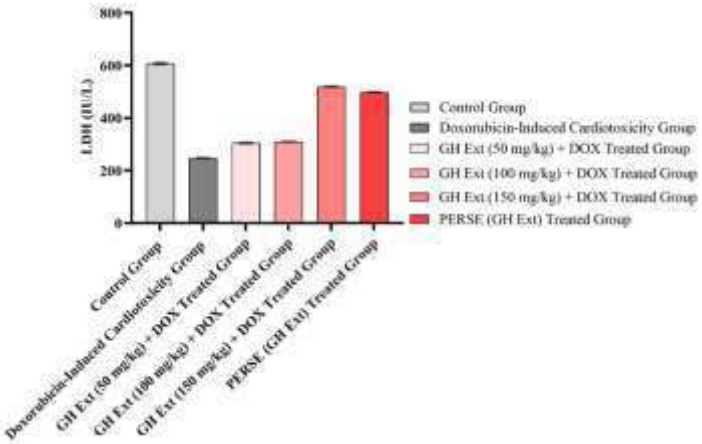

Figure 17: Effect of GHE on changes in LDH

Data was expressed as the mean ± SEM (n=6).

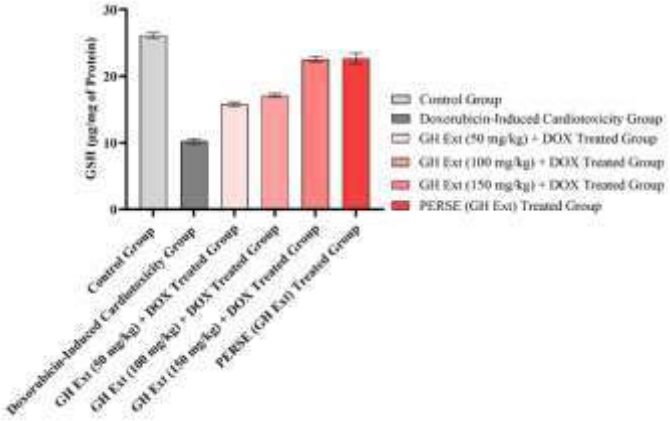

Figure 18: Effect of GHE on changes in GSH

Data was expressed as the mean ± SEM (n=6).

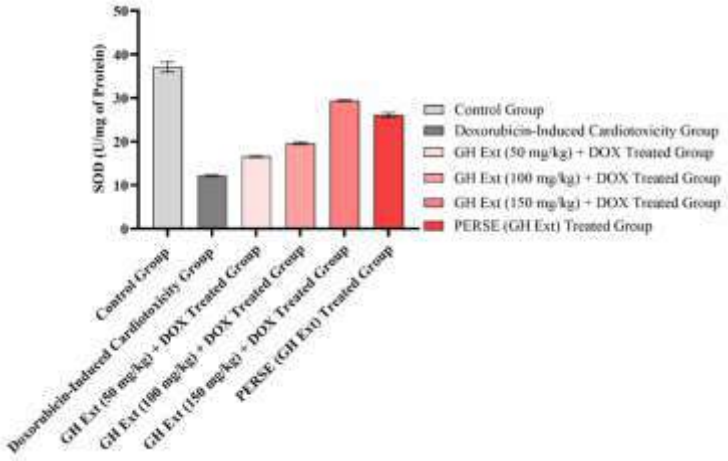

Figure 19: Effect of GHE on changes in SOD

Data was expressed as the mean ± SEM (n=6).

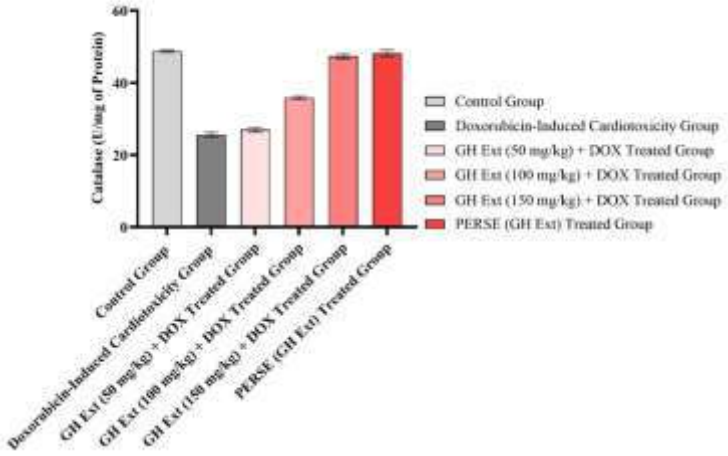

Figure 20: Effect of GHE on changes in catalase

Data was expressed as the mean ± SEM (n=6).

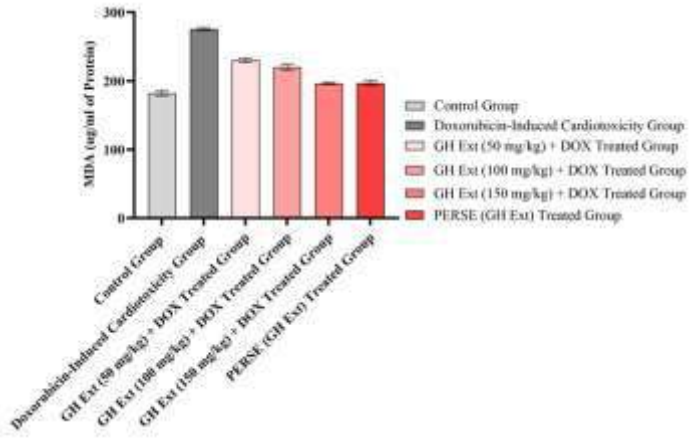

Figure 21: Effect of GHE on changes in MDA

Data was expressed as the mean ± SEM (n=6).

Effect of GHE on changes in NO in doxorubicin induced cardiotoxicity in rats

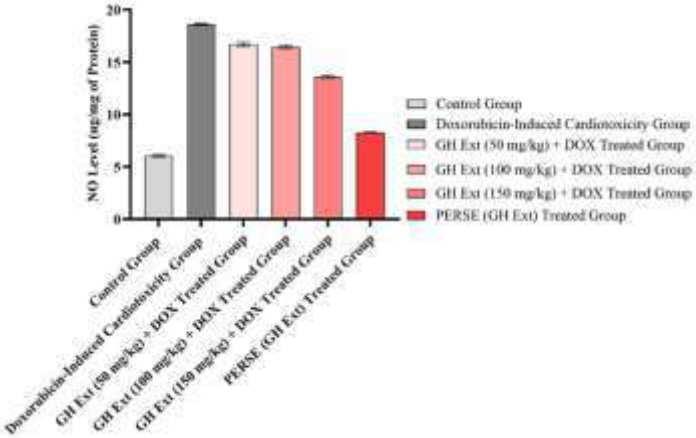

Figure 22: Effect of GHE on changes in NO

Data was expressed as the mean ± SEM (n=6).

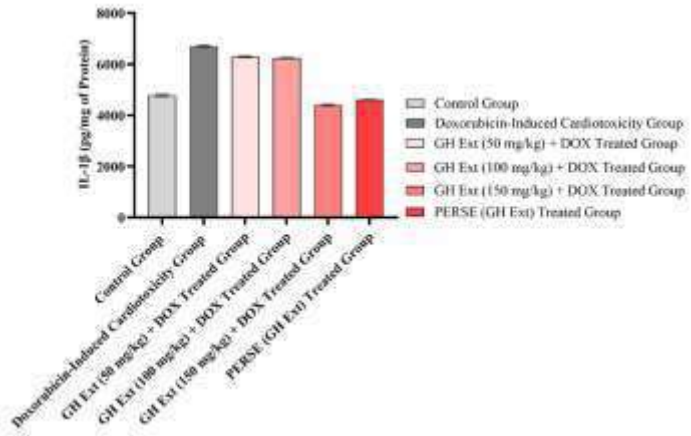

Figure 23: Effect of GHE on changes in IL-1β

Data was expressed as the mean ± SEM (n=6).

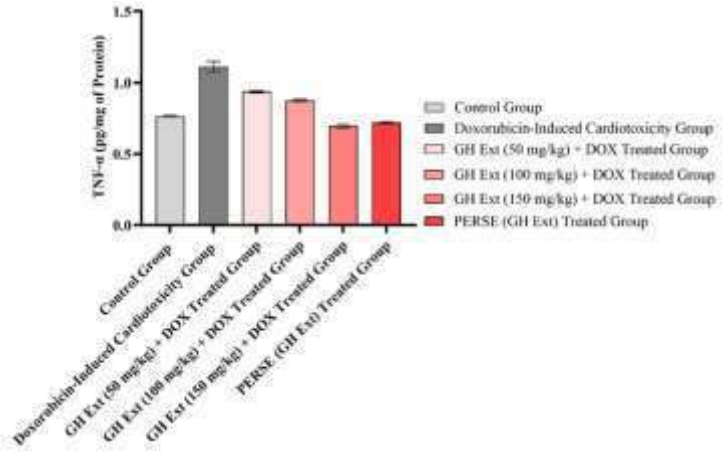

Figure 24: Effect of GHE on changes in TNF-α

Data was expressed as the mean ± SEM (n=6).

HİSTOPATHOLOGİCAL EXAMİNATİON:

The histopathological impact of Grewia hirsuta extract (GHE) at doses of 50, 100, and 150 mg/kg on doxorubicin-induced cardiotoxicity was evaluated in rats using light microscopy, as illustrated in Figure 26 (A–F). The control group (Figure 26A) demonstrated normal myocardial architecture with intact cellular organization. In contrast, the doxorubicin-treated group (Figure 26B) showed marked pathological alterations, including prominent vacuolization, inflammatory infiltration, myofibrillar disruption, and widespread diffuse fibrosis. In the group treated with GHE at 50 mg/kg (Figure 26C), the myocardial damage appeared comparable to that seen in the doxorubicin group, with no significant improvement in histological features. However, administration of 100 mg/kg GHE (Figure 26D) resulted in a noticeable reduction in vacuolization and inflammatory cell infiltration, indicating partial cardioprotection. The group receiving 150 mg/kg GHE in combination with doxorubicin (Figure 26E) exhibited near-normal myocardial architecture, with only minimal vacuolization, suggesting substantial protective effects. Importantly, treatment with GHE alone at 150 mg/kg (Figure 26F) did not produce any structural alterations in cardiac tissue, confirming the extract's safety at this dose.

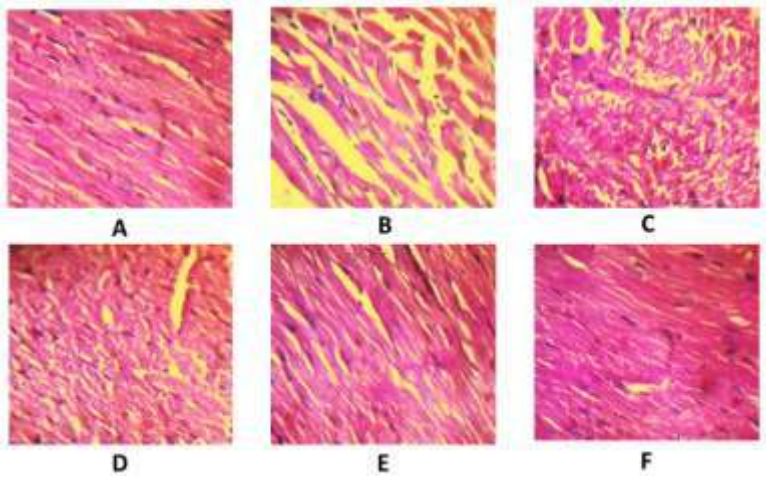

Figure 25: Photomicrograph showing the histoarchitecture changes in the rat myocardium. (A) normal group (H & E, 40 X), (B) doxorubicin (30 mg/kg, i.p) alone (H & E, 40 X), (C-E) GHE (50, 100, 150 mg/kg p.o.) + doxorubicin (30 mg/kg, i.p) respectively (H & E, 40 X), (F) GHE alone (150 mg/kg p.o.) (H & E, 40 X).

NETWORK PHARMACOLOGY

Target Identification and Overlap Analysis

The phytoconstituents identified from Grewia hirsuta leaves—namely (4Z,12Z)-cyclopentadeca-4,12-dienone, Beta-Sitosterol, Gallic acid, Kaempferol, Quercetin, and Caffeic acid—were subjected to target prediction using SwissTargetPrediction and BindingDB. This yielded a total of 363 unique compound-associated targets. Simultaneously, 442 cardiotoxicity-associated genes were curated from GeneCards and DisGeNET using the keyword "Doxorubicin-induced cardiotoxicity." Upon comparison, 67 common genes were identified, representing the pharmacological intersection between the plant's bioactive compounds and cardiotoxicity-related molecular mechanisms (Figure 27). This overlap suggests that the plant extract potentially modulates a subset of disease-relevant proteins, which may be central to its cardioprotective action.

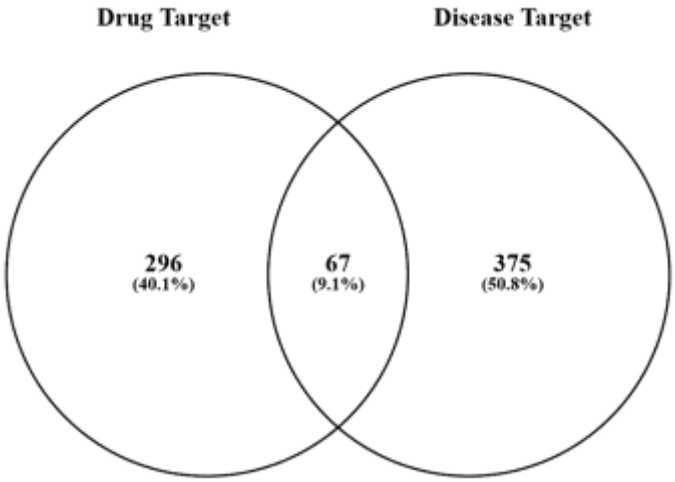

Figure 26: Venn diagram showing the intersection between predicted drug targets from phytoconstituents of Grewia hirsuta and disease targets associated with doxorubicin-induced cardiotoxicity. A total of 67 overlapping genes were identified, indicating the therapeutic target space of the extract.

PROTEİN–PROTEİN INTERACTİON NETWORK:

The 67 intersected targets were used to construct a STRING-based PPI network to elucidate the functional interrelationship between the proteins (Figure 28). The network revealed a densely connected module, with multiple nodes forming interlinked pathways related to oxidative stress regulation, mitochondrial protection, immune response, and cardiac tissue remodeling. These interconnections indicate potential for systems-level modulation by the extract, supporting a polypharmacological mode of action typical of plant-derived therapeutics.

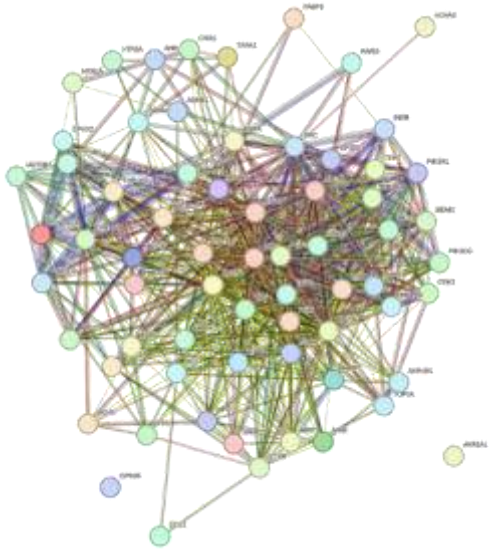

Figure 27: Protein–protein interaction (PPI) network of the 67 overlapping genes constructed using the STRING database. Each node represents a protein, and edges represent predicted functional associations based on multiple evidence types including co-expression and co-occurrence.

Table 3: Top 10 hub genes ranked by degree centrality

Rank	Name	Score
1	AKT1	50
2	ESR1	47
3	PTGS2	44
4	TNF	43
5	BCL2	42
6	STAT3	41
7	EGFR	41
8	SRC	38
9	HIF1A	35
10	ERBB2	35

MOLECULAR DOCKİNG RESULTS :

Table 4: Docking scores of Compounds with respective PBD Ids

Compound	1UUQ	2AZ5	3O96	5F19	5IKV	5KRA	5UUI	7JKW
(4Z,12Z)-cyclopentadeca-4,12-dienone	-	-	-6.81463	-3.60815	-3.71177	-8.65188	-1.14929	-4.58553
Beta-Sitosterol	-1.01128	-1.23371	-	-3.92825		-10.0035	-1.22602	-
Gallic acid	-5.07583	-5.20312	-6.84607	-6.90341	-7.63932	-6.40099	-4.98603	-7.04695
Kaempferol	-2.58445	-3.20896	-8.92213	-6.18133	-5.36279	-10.1997	-5.6504	-9.43196
Quercetin	-4.00554	-4.55838	-10.3491	-6.57945	-5.33234	-10.2956	-6.80331	-10.0093
caffeic acid	-3.94023	-4.42707	-6.177	-7.01862	-7.44091	-7.07244	-4.64808	-7.74829

Table 5: Glide Enegry scores of Compounds with respective PBD Ids

Compound	1UUQ	2AZ5	3O96	5F19	5IKV	5KRA	5UUI	7JKW
(4Z,12Z)-cyclopentadeca-4,12-dienone	-	-	-30.7017	-23.2405	-20.9918	-21.672	-19.7334	-22.4565
Beta-Sitosterol	-16.027	-17.4707	-	-15.8414	-	-3.41507	-11.4146	-
Gallic acid	-17.1673	-22.6531	-25.8083	-21.4301	-25.3425	-24.8793	-25.8399	-27.3448
Kaempferol	-25.6529	-29.7839	-42.3291	-28.8047	-33.6383	-35.617	-31.7156	-44.04
Quercetin	-28.978	-29.2193	-49.9609	-35.17	-35.3194	-34.9675	-35.6558	-46.4424
caffeic acid	-23.7103	-20.4058	-24.6041	-26.6518	-26.9252	-26.9012	-26.9912	-35.4409

Table 6: Best Docking scores and Glide Energy of Compound

Compound	Best Docking Target (PDB)	Docking Score	Glide Energy (kcal/mol)
Quercetin	ESR1 (3O96)	-10.35	-49.96
Kaempferol	EGFR (5KRA)	-10.19	-35.61
Gallic acid	PTGS2 (5KRA)	-6.4	-24.87
Beta-Sitosterol	PTGS2 (5KRA)	-10	-3.41
Caffeic acid	EGFR (5KRA)	-6.88	-24.53
(4Z,12Z)-cyclopentadeca.	EGFR (5KRA)	-8.65	-21.67

PATHWAY ENRİCHMENT ANALYSİS:

Table 7: Pathway enrichment analysis

Term	Category	P-value
PI3K-Akt signaling pathway	KEGG	1.10E-06
TNF signaling pathway	KEGG	3.20E-05
MAPK signaling pathway	KEGG	4.50E-05
HIF-1 signaling pathway	KEGG	7.90E-05
Estrogen signaling pathway	KEGG	0.00013
NF-Î°B signaling pathway	KEGG	0.00022
Apoptosis	KEGG	0.00025
Cytokine–cytokine receptor interaction	KEGG	0.00031
p53 signaling pathway	KEGG	0.00035
Cardiac muscle contraction	KEGG	0.00041

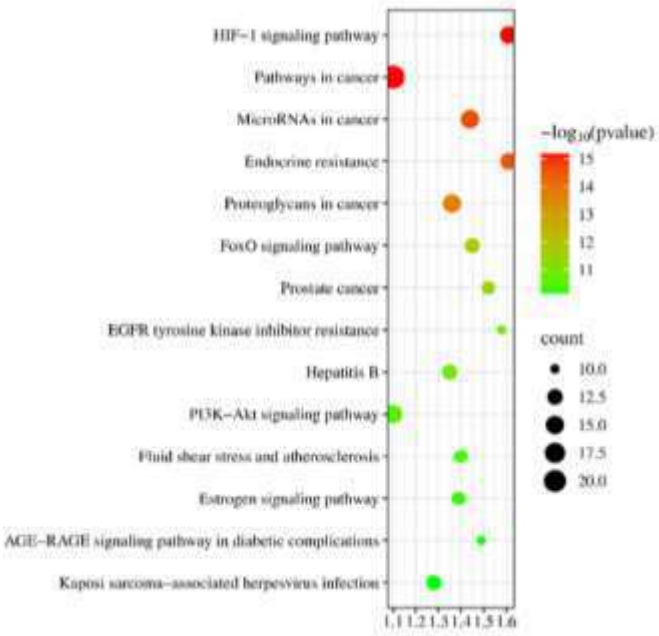

Figure 28: KEGG and GO enrichment bubble plot illustrating the top enriched pathways and biological processes involved in cardioprotection, including PI3K-Akt signaling, TNF signaling, oxidative stress response, and apoptosis regulation.

INTERPRETATİON OF GO TERMS:

Gene Ontology (GO) enrichment analysis provided further insights into the biological processes regulated by the common targets. The term "negative regulation of apoptotic process" was highly enriched and included core genes such as AKT1, BCL2, and HIF1A. This suggests that the extract may help preserve cardiomyocyte viability by preventing mitochondrial-mediated apoptosis, which is a hallmark of Doxorubicin-induced cardiotoxicity.

DİSCUSSİON AND INTERPRETATİON:

The network pharmacology approach applied in this study provides a comprehensive systems-level understanding of the cardioprotective mechanisms underlying the hydroalcoholic extract of Grewia hirsuta leaves. The identification of 67 common targets shared between phytoconstituent-derived and disease-associated genes reveals a significant intersection between the extract's bioactivity and the molecular pathology of Doxorubicin-induced cardiotoxicity. The dense interconnectivity observed within the PPI network reinforces the hypothesis that the extract functions through synergistic interactions across multiple biological modules rather than through a single-target effect.

The hub genes identified, such as AKT1, PTGS2, ESR1, STAT3, and HIF1A, reflect critical nodes in cardiac pathophysiology. For instance, AKT1 activation promotes cell survival and limits Doxorubicin-induced apoptosis, while PTGS2 plays a dual role by participating in prostaglandin-mediated inflammation and vascular homeostasis. The identification of ESR1 and HIF1A further highlights the extract's influence on hormonal and hypoxic responses in the myocardium. This indicates that the cardioprotective effect of Grewia hirsuta is not only anti-inflammatory and anti-apoptotic in nature but also encompasses broader regulatory control over oxidative stress and vascular adaptation.

The strong docking interactions of Quercetin and Kaempferol with multiple hub proteins confirm the plausibility of physical and functional

interactions at the molecular level. The enrichment of key signaling pathways such as PI3K-Akt, TNF, and MAPK further supports the extract's multi-dimensional modulation of pathways associated with myocardial injury, immune activation, and cell survival. Importantly, the enrichment of the Estrogen and HIF-1 signaling pathways underscores the relevance of this extract in modulating responses to oxidative damage and ischemia—two primary factors in Doxorubicin-induced cardiac dysfunction. Moreover, the extract's potential involvement in the NF-κB and p53 signaling pathways suggests its role in modulating transcriptional responses to DNA damage, cytokine signaling, and cell cycle arrest. These are often triggered by chemotherapeutic agents like Doxorubicin. The presence of genes related to cardiac muscle contraction in the pathway enrichment indicates that the extract may also have a direct role in supporting myocardial function and electrophysiological stability. Taken together, the evidence demonstrates that the phytoconstituents of Grewia hirsuta engage a complex network of targets and pathways, collectively supporting antioxidant defense, suppression of inflammation, inhibition of apoptosis, and promotion of cell survival and tissue regeneration. These insights not only justify the ethnopharmacological use of this plant in cardiovascular disorders but also lay the groundwork for further pharmacological, toxicological, and formulation studies aimed at its therapeutic development.

CONCLUSION:

The current study elucidates the significant cardioprotective potential of Grewia hirsuta hydroalcoholic extract against doxorubicin-induced cardiotoxicity through a multifaceted mechanism involving antioxidant, anti-inflammatory, and membrane-stabilizing effects. Hemodynamic disturbances induced by DOX, such as elevated systolic (121.63 mmHg) and diastolic pressures (81.45 mmHg), as well as increased heart rate (403.41 bpm), were effectively normalized by EXT administration (113.91 mmHg, 71.78 mmHg, and 373.55 bpm respectively for 40 mg/kg dose). Biochemical markers of cardiac injury, such as CK-MB and LDH, were significantly restored in EXT-treated rats, indicating myocardial preservation. Oxidative stress markers like MDA, GSH, SOD, and catalase demonstrated profound improvement, suggesting that EXT neutralized free radicals and re-established redox balance. Furthermore, inflammatory cytokines TNF-α and IL-1β were downregulated by EXT, reducing the inflammatory burden associated with cardiotoxicity. The synergistic effect of multiple phytoconstituents in Grewia hirsuta likely contributed to these outcomes. The computational modeling aligned well with the experimental data, confirming potential protein targets involved in cardioprotection. Therefore, Grewia hirsuta extract exhibits significant therapeutic promise for mitigating DOX-induced cardiac damage, supporting its ethnomedicinal use and offering a scientific foundation for its future development as an adjuvant or standalone cardioprotective agent. Further studies involving isolation of bioactive constituents, in-depth mechanistic pathways, and clinical validations are warranted to translate these findings into clinical applications. Nevertheless, this integrative approach combining computational insights and experimental validation provides compelling evidence for the cardioprotective efficacy of Grewia hirsuta.

ACKNOWLEDGEMENT:

In this research the authors are sincerely acknowledge the valuable contributions of all previous researchers whose work has provided

valuable insight for understanding the traditional uses, phytochemistry and preliminary studies of Grewia hirsuta. We express our sincere thanks to our respective institutions for providing the necessary support and resources to carry this research. Special thanks to the library that facilitated access to the extensive scientific literature used in this research.

REFERENCES

1. Agrawal, H., Choy, H.H.K., Liu, J., Auyoung, M., Albert, M.A., 2020. Coronary Artery Disease. Arterioscler. Thromb. Vasc. Biol. 40, E185–E192. https://doi.org/10.1161/ATVBAHA.120.313608
2. Anderson, R.H., Razavi, R., Taylor, A.M., 2004. Cardiac anatomy revisited. J. Anat. 205, 159–177. https://doi.org/10.1111/j.0021-8782.2004.00330.x
3. Article, R., 2016. Coronary-Artery Bypass Grafting. https://doi.org/10.1056/NEJMra1406944
4. Athyros, V.G., Mikhailidis, D.P., Papageorgiou, A.A., Bouloukos, V.I., Pehlivanidis, A.N., Symeonidis, A.N., Elisaf, M., 2004. Effect of statins and ACE inhibitors alone and in combination on clinical outcome in patients with coronary heart disease. J. Hum. Hypertens. 18, 781–788. https://doi.org/10.1038/sj.jhh.1001748
5. Begum, M.M., Alim, M.A., Ahmed, M.R., Mamun, A. Al, Das, M., Begum, R., Islam, A., Moni, M.M.R., Alam, S., Akter, W., Rahman, M.S., 2021. Rudimentary Pharmacological Inspection of the Ethanolic Extract of Grewia hirsute Vhal. J. Pharm. Res. Int. 33, 10–26. https://doi.org/10.9734/jpri/2021/v33i43b32520
6. Chikkamath, V., Kulkarni, V.H., Habbu, P. V., Nagappa, A.N., 2022. Grewia hirsuta Vahl. Hydroethanolic Leaf Extract: Phytochemical and Acute Toxicological Studies. J. Pharm. Sci. 12, 23–30. https://doi.org/10.1002/jps.21263
7. Chikkamath, V., Kulkarni, V.H., Habbu, P. V., Nagappa, A.N., Sindhu, G.M., 2024. ANTIOXIDANT AND CHOLINESTERASE INHIBITORY ACTIVITY OF GREWIA HIRSUTA VAHL. LEAVES V. IJPSR 15, 37–48. https://doi.org/10.13040/IJPSR.0975-8232.15(8).2495-99
8. Das, M., Debnath, D., Hoque, M.A., Rahman, M.S., Alam, S., Islam, A., Begum, M.M., 2019. Preliminary phytochemical and biological investigations of ethanolic extract of Grewia hirsute Vahl. Orient. Pharm. Exp. Med. 19, 145–156. https://doi.org/10.1007/s13596-019-00371-3
9. Dolci, G.E.F., Anda, F.J.V.-D., Ortiz-Vázquez, P., Olaiz-Fernández, G., 2024. The burden of cardiovascular disease in Mexico 1990-2021. Summary of the Global Burden of Disease 2021 study. Gac. Med. Mex. https://doi.org/10.24875/gmm.m24000837
10. Dong, J., Zhang, Z., Sun, J., Yang, X., Zhang, W., 2024. The cardiovascular disease burden attributable to kidney dysfunction from 1990 to 2021: an age-period-cohort analysis of the Global Burden of Disease study. Eur. Hear. J. - Qual. Care Clin. Outcomes. https://doi.org/10.1093/ehjqcco/qcae088
11. Edwards, W.D., 1987. Cardiomyopathies. Hum. Pathol. 18, 625–635. https://doi.org/10.1016/S0046-8177(87)80364-7
12. Ellis, H., 2012. The anatomy of the heart. Anaesth. Intensive Care Med. 13, 355–357. https://doi.org/10.1016/j.mpaic.2012.05.003
13. Ema, A., Kumar, M.S., Rebecca, L.J., Sindhu, S., Anbarasi, P., Sagadevan, E., Arumugam, P., 2013. Evaluation of Antiproliferative effect of Grewia hirsuta on HepG2 cell lines. J. Acad. Ind. Res. 2, 1–5.

14. Fathallah, M., Krasuski, R.A., 2017. Pulmonic Valve Disease: Review of Pathology and Current Treatment Options. Curr. Cardiol. Rep. 19. https://doi.org/10.1007/s11886-017-0922-2
15. Fathima, N.S., 2021. Current Research and Trends in Medical Science and Technology- An update on myocardial infarction.
16. Faust, O., Martis, R.J., Min, L., Zhong, G.L.Z., Yu, W., 2013. Cardiac arrhythmia classification using electrocardiogram. J. Med. Imaging Heal. Informatics 3, 448–454. https://doi.org/10.1166/jmihi.2013.1179
17. Ferrão De Oliveira, J.M., Antunes, M.J., 2006. Mitral valve repair: Better than replacement. Heart 92, 275–281. https://doi.org/10.1136/hrt.2005.076208
18. Ferrer, M.I., 1973. Cardiac Arrhythmias The Sick Sinus Syndrome. Circulation XLVII, 635–641.
19. Garg, S., Hasija, S., Sharma, P., Kalhan, S., Saini, N., Khan, A., 2018. A histopathological analysis of prevalence of various heart diseases: an autopsy study. Int. J. Res. Med. Sci. 6, 1414. https://doi.org/10.18203/2320-6012.ijrms20181306
20. González, A., Fortuño, M.A., Querejeta, R., Ravassa, S., López, B., López, N., Díez, J., 2003. Cardiomyocyte apoptosis in hypertensive cardiomyopathy. Cardiovasc. Res. 59, 549–562. https://doi.org/10.1016/S0008-6363(03)00498-X
21. Gregg, D.E., 1960. Physiology of the Coronary Circulation. Ann. N. Y. Acad. Sci. 90, 145–155. https://doi.org/10.1111/j.1749-6632.1960.tb32628.x
22. Guthrie, R.B., Vlodaver, Z., Nicoloff, D.M., Edwards, J.E., 1975. Pathology of stable and unstable angina pectoris. Circulation 51, 1059–1063. https://doi.org/10.1161/01.CIR.51.6.1059
23. Hanson, M.A., Fareed, M.T., Argenio, S.L., Agunwamba, A.O., Hanson, T.R., 2013. Coronary Artery Disease. Prim. Care - Clin. Off. Pract. 40, 1–16. https://doi.org/10.1016/j.pop.2012.12.001
24. Jaiswal, M.M., C.K.Tyagi, D., Budholiya, D.P., 2021. EVALUATION OF BIOACTIVE CONSTITUENTS AND IN-VIVO ANTI-INFLAMATORY ACTIVITY OF HYDROALCOHOLIC LEAVES EXTRACT OF GREWIA HIRSUTA. J. Biomed. Pharm. Res. 4, 127–150.
25. Jawad, E., Arora, R., 2008. Chronic Stable Angina Pectoris. Disease-a-Month 54, 671–689. https://doi.org/10.1016/j.disamonth.2008.06.009
26. Kashyap, R., Mohammed, J.S., Singh, A., Sharma, A.K., Sukhramani, P.S., 2025. Ethnopharmacological Insights into the Role of Medicinal Plants in Cardiovascular Health 1, 9–14.
27. Kature, D., Gupta, G., Gilotra, R., 2020a. Phytochemical Investigation & Antibacterial Activity of Hydroethanolic Leaf Extract of Grewia Hirsuta Collected From Forest. J. Pharm. Res. Educ. 2020, 423–431.
28. Kature, D., Gupta, G., Gilotra, R., 2020b. Phytochemical evaluation, HPTLC analysis and in-vitro antioxidant activity of hydroalcoholic leaf extract of Grewia hirsuta collected fromWestern Ghats forest. Int. J. Res. Pharm. Sci. 11, 4653–4659.
29. Kemp, C.D., Conte, J. V., 2012. The pathophysiology of heart failure. Cardiovasc. Pathol. 21, 365–371. https://doi.org/10.1016/j.carpath.2011.11.007
30. Kumar, S., Singh, B., Bajpai, V., 2022. Traditional uses, phytochemistry, quality control and biological activities of genus Grewia. Phytomedicine Plus 2, 100290. https://doi.org/10.1016/j.phyplu.2022.100290

31. Maganti, K., Rigolin, V.H., Sarano, M.E., Bonow, R.O., 2010. Valvular heart disease: Diagnosis and management. Mayo Clin. Proc. 85, 483–500. https://doi.org/10.4065/mcp.2009.0706
32. Marijon, E., Mirabel, M., Celermajer, D.S., Jouven, X., 2012. Rheumatic heart disease. Lancet 379, 953–964. https://doi.org/10.1016/S0140-6736(11)61171-9
33. Martín-Fernández, B., Gredilla, R., 2016. Mitochondria and oxidative stress in heart aging. Age (Omaha). 38, 225–238. https://doi.org/10.1007/s11357-016-9933-y
34. Miller, L., Birks, E., Guglin, M., Lamba, H., Frazier, O.H., 2019. Use of Ventricular Assist Devices and Heart Transplantation for Advanced Heart Failure. Circ. Res. 124, 1658–1678. https://doi.org/10.1161/CIRCRESAHA.119.313574
35. Minhas, A.M., Sedhom, R., Jean, E.D., Shapiro, M.D., Panza, J.A., Alam, M., Virani, S.S., Ballantyne, C., Abramov, D., 2024. Global burden of cardiovascular disease attributable to smoking, 1990-2019: an analysis of the 2019 Global Burden of Disease Study. Eur. J. Prev. Cardiol. https://doi.org/10.1093/eurjpc/zwae040
36. Mori, S., Spicer, D.E., Anderson, R.H., 2015. Revisiting the anatomy of the living heart. Circ. J. 80, 24–33. https://doi.org/10.1253/circj.CJ-15-1147
37. Morton, P.G., 2012. Acute myocardial infarction. Crit. Care Nurs. A Holist. Approach 10th Ed. 417–443. https://doi.org/10.1056/NEJMra1606915
38. Muharram, F.R., Multazam, C.E.C.Z., Mustofa, A., Socha, W., Andrianto, Martini, S., Aminde, L., Yi-Li, C., 2024. The 30 Years of Shifting in The Indonesian Cardiovascular Burden—Analysis of The Global Burden of Disease Study. J. Epidemiol. Glob. Health. https://doi.org/10.1007/s44197-024-00187-8
39. MURPHY, F.D., 1947. Hypertensive heart disease. J. Mich. State Med. Soc. 46, 310–317.
40. Natarajan, A., Sugumar, S., Bitragunta, S., Balasubramanyan, N., 2015. Molecular docking studies of (4Z, 12Z)-cyclopentadeca-4, 12-dienone from Grewia hirsuta with some targets related to type 2 diabetes. BMC Complement. Altern. Med. 15, 1–8. https://doi.org/10.1186/s12906-015-0588-5
41. Newman, J.H., 2005. Pulmonary hypertension. Am. J. Respir. Crit. Care Med. 172, 1072–1077. https://doi.org/10.1164/rccm.200505-684OE
42. Raines, L., 2023. Atrial Arrhythmias. Cardiovasc. Man. Adv. Pract. Provid. Mastering Basics 324, 91–111. https://doi.org/10.1007/978-3-031-35819-7_9
43. Ramanathan, T., Skinner, H., 2005. Coronary blood flow. Contin. Educ. Anaesthesia, Crit. Care Pain 5, 61–64. https://doi.org/10.1093/bjaceaccp/mki012
44. Reddy, K.S., Reddy, K.S., Mathur, M.R., Mathur, M.R., 2021. Global Burden of CVD: Prevalence, Pattern and Trends. null. https://doi.org/10.1007/978-3-030-05325-3_24-1
45. Singh, V., Martinezclark, P., Pascual, M., Shaw, E.S., O'Neill, W.W., 2010. Cardiac biomarkers - The old and the new: A review. Coron. Artery Dis. 21, 244–256. https://doi.org/10.1097/MCA.0b013e328338cd1f
46. Sk, S., Sharma, S., Sarnak, M.J., Sarnak, M.J., 2017. Epidemiology: The global burden of reduced GFR: ESRD, CVD and mortality. Nat. Rev. Nephrol. https://doi.org/10.1038/nrneph.2017.84
47. Wilson, B.H., Poh, K.K., 2023. Addressing the Global Burden of CVD Through

"ACCelerated" Action. J. Am. Coll. Cardiol. https://doi.org/10.1016/j.jacc.2023.05.015

HOW TO CITE: Aditi Malkar, Karna Khavane, Aditi Jyotishi, Decoding the Cardioprotective Effects of Grewia hirsuta: A Computational and Experimental Approach, Int. J. of Pharm. Sci., 2025, Vol 3, Issue 7, 3835-3866. https://doi.org/10.5281/zenodo.16537277